J. Fluid Mech. (1994), *vol.* 272, *pp.* 91–107

Steady, viscous, free-surface flow on a rotating cylinder

By ERIK B. HANSEN[1] AND MARK A. KELMANSON[2]

[1] Mathematical Institute, Technical University of Denmark, DK-2800 Lyngby, Denmark

[2] Department of Applied Mathematical Studies, University of Leeds, Leeds LS2 9JT, UK

(Received 19 August 1993 and in revised form 13 January 1994)

The commonly observed phenomenon of steady, viscous, free-surface flow on the outer surface of a rotating cylinder is investigated by means of an iterative, integral-equation formulation applied to the Stokes approximation of the Navier–Stokes equations. The method of solution places no restriction on the thickness of the fluid layer residing on the cylinder surface; indeed, results are presented for cases where the layer thickness is of the same order of magnitude as the cylinder radius.

Free-surface profiles and free-surface velocity distributions are presented for a range of flow parameters. Where appropriate, comparisons are made with the results of thin-film theory; excellent agreement is observed.

For all film thicknesses and surface tensions, results show a high degree of symmetry about a horizontal axis even though the gravity field is vertical. A proof is presented that, for vanishing surface tension, this is a consequence of the Stokes approximation.

1. Introduction

It is a well-known phenomenon that, if a knife is dipped in a viscous liquid (such as syrup) and rotated about a horizontal axis, a certain amount of the liquid can be made to remain on the knife as a result of the balance between competing actions of gravity, the rotation of the knife, and the viscous forces within the liquid. Intuition suggests that the directional, viscous forces generated in a liquid by the rotation of a circular cylinder might balance the draining force of gravity to give rise to a steady, two-dimensional flow possessing a free surface of stationary profile.

Beginning with the case of infinite viscosity, in which the fluid volume moves as a rigid body with the cylinder, Pukhnachev (1974, 1977) used contraction mapping techniques to prove the existence of a steady-state solution of the Navier–Stokes equations for problems in which part of the fluid domain was bounded by a moving, rigid surface, and part by a free surface. Moffatt (1977) studied the problem in the thin-film régime and found an approximate expression for the maximum load. Using kinematic wave theory, Moffatt (1977) proceeded to investigate the onset of instabilities; he also performed experiments with which to compare his theoretical results. Using a thin-film theory, Preziosi & Joseph (1988) confirmed Moffatt's maximum-load condition and performed experiments which they too compared with theory.

In §2, we consider the problem in the Stokes approximation. This approximation may be justified by noting that, for the water–syrup mixture used in Moffatt's (1977) experiments, the dynamic viscosity, μ, was approximately 80 g cm^{-1} s^{-1}. Thus, with a

density, ρ, of approximately 1 g cm^{-3}, and a radius, a, of 1 cm, the Reynolds number, defined as $R \equiv \rho a^2 \omega/\mu$, is of the order 10^{-1}, even for ω as high as 2π s^{-1} (i.e. one revolution per second).

Since the flow is incompressible, a biharmonic stream function may be introduced, as in §2, to formulate the problem as an integral equation over the free surface. In classical biharmonic problems, two boundary conditions suffice but, since the location of the free surface is here *a priori* unknown, three boundary conditions have to be applied thereon; one each for normal and shear stress, and one reflecting zero flux across the (stationary-profile) surface. In §3 we present a derivation of an integral-equation formulation, as well as a summary of the subsequent numerical solution procedure. Section 4 contains a discussion of results obtained from the integral-equation approach, some of which are compared with those obtained from thin-film theory.

One advantage of the integral-equation formulation presented here is that there is no restriction on the thickness of the fluid layer which can be so investigated, hence we are able to extend our parameters beyond those of the thin-film régime. However, we make no attempt here to discuss results for high rotation rates since we know, from the experimental evidence of Moffatt (1977), that, as ω is increased, surface instabilities appear and the flow ceases to be even approximately two-dimensional.

We conclude this section by remarking that, far from being a purely mathematical exercise, this problem is motivated by the very real applications inherent in a multitude of industrial roller-coating processes. Moffatt (1977) gives a brief summary of the potential areas of application, and Malone (1992) and Thompson (1992) give extensive and up-to-date résumés of experimental, theoretical and numerical work in this field.

2. Governing equations and boundary conditions

We consider a circular cylinder of radius a which rotates about a horizontal axis with a constant angular velocity ω. The cylinder is covered by an annular layer of viscous fluid. We wish to find the motion of the fluid and, in particular, the shape of the stationary fluid surface when the motion is steady.

We assume that the fluid is incompressible, that the Stokes approximation is applicable, and that there is no flow in the axial direction. Under these assumptions, the flow is two-dimensional. If the curves C and S are those representing respectively the cylinder and free surface (see figure 1), then the flow in the annular region between them can be expressed in terms of a stream function, ψ, with corresponding velocity field $\boldsymbol{v} = (\partial\psi/\partial y,\ -\partial\psi/\partial x)$.

With the y-axis vertical, the equations of motion are

$$\frac{\partial p}{\partial x} = \mu \frac{\partial \Delta\psi}{\partial y}, \quad \frac{\partial p}{\partial y} = -\mu \frac{\partial \Delta\psi}{\partial x} - \rho g, \tag{2.1}$$

where p is the pressure, g the acceleration due to gravity, ρ the density, and μ the dynamic viscosity of the fluid. On S, the stream function is a constant and, since the velocity field determines ψ only to within an arbitrary additive constant, we set $\psi = 0$ on S. Furthermore, the shear stress vanishes on S and the normal stress there is due solely to surface tension. Under the stream-function formulation, these two facts are expressed by the conditions

$$\frac{\partial^2 \psi}{\partial T^2} - \frac{\partial^2 \psi}{\partial N^2} = 0, \quad -p + 2\mu \frac{\partial^2 \psi}{\partial T \partial N} = \sigma\kappa. \tag{2.2}$$

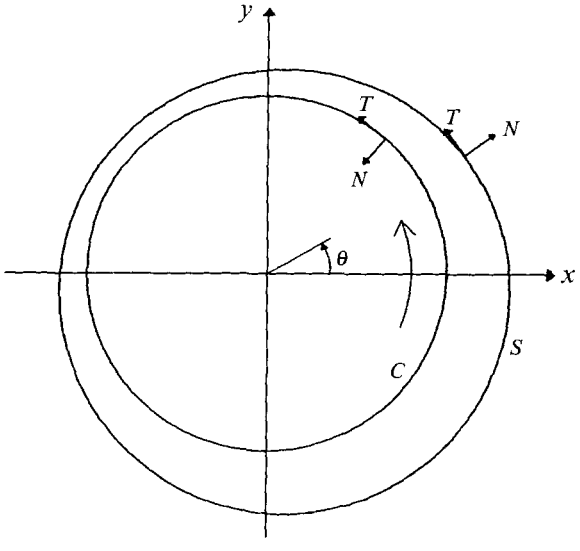

FIGURE 1. A circular cylinder, covered by a layer of viscous liquid, rotating in the direction of the arrow.

Here $\partial/\partial T$ and $\partial/\partial N$ denote differentiation with respect to Cartesian coordinates in the directions of the tangent and outward normal (see figure 1), σ is the surface tension, and κ is the curvature of S, κ being positive if the centre of curvature is in the direction of the outward normal. On C, the stream function also assumes a constant value, and the no-slip condition requires the fluid velocity there to equal that of the roller surface. Thus, with $\partial/\partial N$ denoting differentiation in the direction of the normal pointing into the cylinder, the boundary conditions on $C(r = a)$ are

$$\psi = \text{constant}, \quad \frac{\partial \psi}{\partial N} = \omega a. \tag{2.3}$$

We non-dimensionalize the above equations using the cylinder radius a as the lengthscale, ωa as the unit of velocity, and $\omega\mu$ as the unit of stress. In the ensuing analysis, non-dimensional variables are represented by the same symbols as those with dimensions. The non-dimensional equations of motion are

$$\frac{\partial p}{\partial x} = \frac{\partial \Delta \psi}{\partial y}, \quad \frac{\partial p}{\partial y} = -\frac{\partial \Delta \psi}{\partial x} - \gamma, \tag{2.4}$$

with boundary conditions

$$\left.\begin{aligned} \psi = 0, \quad & \frac{\partial^2 \psi}{\partial T^2} - \frac{\partial^2 \psi}{\partial N^2} = 2\frac{\partial^2 \psi}{\partial T^2} - \Delta\psi = 0, \\ & -p + 2\frac{\partial^2 \psi}{\partial T \partial N} = \alpha\kappa, \end{aligned}\right\} \tag{2.5}$$

on S, and

$$\psi = \psi_0, \quad \frac{\partial \psi}{\partial N} = 1, \tag{2.6}$$

on C. The non-dimensional surface tension α and acceleration due to gravity γ are given by

$$\alpha = \frac{\sigma}{\omega\mu a}, \quad \gamma = \frac{\rho g a}{\omega\mu}. \tag{2.7}$$

If the total fluid mass per unit length of the cylinder is given, the total fluid flux, ψ_0, in (2.6) is not known *a priori*. However, it can of course be evaluated when the flow in the fluid annulus has been determined. Conversely, if ψ_0 is given, the total mass per unit length of the cylinder is *a priori* unknown, but can be computed once the solution has been obtained. In our integral-equation approach to the problem it is convenient to choose the latter alternative.

3. Integral-equation formulation

The problem defined in §2 is solved by means of an integral-equation method similar to one previously applied by Hansen (1987), who used an integral formula for the stream function, incorporating all of the boundary conditions, to establish a Fredholm integral equation of the second kind with only one unknown, namely the tangential fluid velocity on the free surface, v_T.

In the equation for v_T, the integral is taken along the curves C and S introduced in the previous section. With a suitable choice of Green function, certain contributions to the integral along C can be evaluated exactly, while others can be annihilated, thus leaving us with a formula for the stream function expressed in terms of an integral, along S, containing v_T. From that formula, we derive an integral equation for v_T on S. In order to solve the integral equation for v_T, we must specify an initial approximation, $S^{(0)}$, to the *a priori* unknown S. Solution of this equation gives us, in an obvious notation, a solution function, $v_T^{(0)}$, which we then insert into the integral formula for the stream function which, via (2.5), should vanish on S. However, at a chosen set of collocation points on $S^{(0)}$, ψ will not (in general) vanish; these non-zero values are used to obtain a new approximation, $S^{(1)}$, to S. The iterative process is repeated until a surface $S^{(m)}$, $m \in \mathbb{N}$, is obtained for which $|\psi| \leqslant \epsilon$ at all collocation points on $S^{(m)}$, for some prespecified tolerance $\epsilon > 0$.

We begin with the formula

$$\psi(\boldsymbol{r}') = \int_{\partial\Omega} \left\{ \frac{\partial \Delta\psi}{\partial N} G - \Delta\psi \frac{\partial G}{\partial N} + \frac{\partial \psi}{\partial N} \Delta G - \psi \frac{\partial \Delta G}{\partial N} \right\} \mathrm{d}s, \tag{3.1}$$

which expresses the value of a biharmonic function ψ at an arbitrary point $\boldsymbol{r}'$ in a region Ω, with boundary $\partial\Omega$, in terms of ψ and its derivatives on $\partial\Omega$. In (3.1), $\boldsymbol{r}' \in \Omega$ and $G = G(\boldsymbol{r}', \boldsymbol{r})$ is a fundamental solution of the biharmonic equation which we further require to vanish, along with its normal derivative, on C. (If $\boldsymbol{r}' \in \partial\Omega$, a factor $\frac{1}{2}$ multiplies the left-hand side of (3.1).) All functions of ψ are evaluated at $\boldsymbol{r} \in \partial\Omega$, and $\mathrm{d}s = \mathrm{d}s(\boldsymbol{r})$.

Of course, several such fundamental solutions (with different behaviour at infinity) exist; they can be found by using separation of variables and subsequently summing the Fourier series in order to express the solutions in closed form. We chose to use the fundamental solution given by

$$G(\boldsymbol{r}', \boldsymbol{r}) = -\frac{1}{16\pi} \left\{ |\boldsymbol{r}' - \boldsymbol{r}|^2 \ln \frac{r'^2 |\boldsymbol{r}'' - \boldsymbol{r}|^2}{|\boldsymbol{r}' - \boldsymbol{r}|^2} - (r'^2 - 1)(r^2 - 1) \right\}, \tag{3.2}$$

where $r = |\boldsymbol{r}|$, $r' = |\boldsymbol{r}'|$, and $\boldsymbol{r}'' = \boldsymbol{r}'/r'^2$. One may verify that $G = \partial G/\partial r = 0$ on $r = 1$.

We apply (3.1) with $\partial\Omega = C \cup S$, and the stream function inserted for ψ, in which case the integral is equal to $\psi(\boldsymbol{r}')$ for an arbitrary point $\boldsymbol{r}'$ within the fluid region. We now use the fact that G and its normal derivative vanish on C, together with boundary conditions (2.6), to find that the contribution to the stream-function integral from the cylinder surface is

$$\int_C \left\{\Delta G - \psi_0 \frac{\partial \Delta G}{\partial N}\right\} \mathrm{d}s, \tag{3.3}$$

which, upon using (3.2), we may evaluate exactly to be

$$\tfrac{1}{2}(1-r'^2)+\psi_0. \tag{3.4}$$

Since $\psi = 0$ on S, the last term in the integral in (3.1), taken along S, vanishes. With the directions of the tangent and normal vectors on S as shown in figure 1, the equations of motion imply that

$$\int_S \frac{\partial \Delta\psi}{\partial N} G \,\mathrm{d}s = -\int_S \left\{\frac{\partial p}{\partial s} + \gamma T_y\right\} G \,\mathrm{d}s, \tag{3.5}$$

where T_y is the y-component of the tangent vector. In order to rewrite the integral of the remaining terms we express the derivatives, used in (2.2), in terms of derivatives with respect to the free-surface arc length s and the normal direction:

$$\frac{\partial^2 f}{\partial T \partial N} = \frac{\partial}{\partial s}\left(\frac{\partial f}{\partial N}\right) + \kappa \frac{\partial f}{\partial s}, \tag{3.6}$$

$$\frac{\partial^2 f}{\partial T^2} = \frac{\partial^2 f}{\partial s^2} - \kappa \frac{\partial f}{\partial N}. \tag{3.7}$$

Here, f is any twice-differentiable function. We now apply the normal stress condition on S, use (3.6) and integrate by parts to rewrite (3.5) as

$$\int_S \frac{\partial \Delta\psi}{\partial N} G \,\mathrm{d}s = -\int_S \left\{2\frac{\partial^2 G}{\partial s^2}\frac{\partial \psi}{\partial N} + \alpha\kappa \frac{\partial G}{\partial s} + \gamma T_y G\right\} \mathrm{d}s. \tag{3.8}$$

Applying the shear stress condition on S, together with (3.7), we find the second term in the integral in (3.1) to be

$$-\int_S \Delta\psi \frac{\partial G}{\partial N} \mathrm{d}s = \int_S 2\kappa \frac{\partial \psi}{\partial N}\frac{\partial G}{\partial N} \mathrm{d}s. \tag{3.9}$$

Combining the expressions for the various terms in the integral in (3.1) and using (3.7) once more, we obtain the following integral formula for the stream function at an arbitrary point in the fluid region:

$$\psi(\boldsymbol{r}') = \tfrac{1}{2}(1-r'^2)+\psi_0 + \int_S \left\{\left[\frac{\partial^2 G}{\partial T^2} - \frac{\partial^2 G}{\partial N^2}\right] v_T - \alpha\kappa \frac{\partial G}{\partial s} - \gamma T_y G\right\} \mathrm{d}s. \tag{3.10}$$

In (3.10), the unknown $v_T \equiv -\partial\psi/\partial N$ is the tangential fluid velocity, in the anticlockwise direction, at the fluid surface.

We can now derive an integral equation for v_T by taking the derivative of both sides of (3.10), with respect to the primed coordinates, in the direction of the normal to S at a point $\boldsymbol{r}_0 \in S$. Thereafter, we let $\boldsymbol{r}'$ approach $\boldsymbol{r}_0$ to obtain the following Fredholm equation of the second kind,

$$\tfrac{1}{2}v_T(s') + \int_S \frac{\partial}{\partial N'}\left[\frac{\partial^2 G}{\partial T^2} - \frac{\partial^2 G}{\partial N^2}\right] v_T(s)\,\mathrm{d}s = \boldsymbol{r}' \cdot \boldsymbol{N}' + \int_S \left\{\alpha\kappa \frac{\partial}{\partial N'}\left[\frac{\partial G}{\partial s}\right] + \gamma T_y \frac{\partial G}{\partial N'}\right\}\mathrm{d}s. \quad (3.11)$$

Equation (3.11) holds for all $s' \in S$.

In the numerical solution procedure, we find the position of the boundary S and surface velocity v_T by means of an iterative, minimax optimization method developed by Madsen (1975) and implemented in the Fortran routine MIOINF described in Madsen, Hegelund & Hansen (1991). First $S^{(0)}$, an initial approximation to S, is chosen. A set of collocation points are uniformly distributed along $S^{(0)}$, which points are free to move along the normals to $S^{(0)}$ during the optimization process. Subsequent approximations, $S^{(m)}$ $(m \geqslant 1)$, are defined by the displaced collocation points. The tangent and curvature of the current approximation $S^{(m)}$ are taken as those of the circle passing through the updated collocation point and its immediate neighbours. In between collocation points, $S^{(m)}$ is represented by quadratic parameterization. The unknown free-surface velocity is approximated by a continuous function which is linear between collocation points.

The described discretization of the original integral equations yields a system of linear algebraic equations in which the number of unknowns is equal to the number of collocation points. The elements of the coefficient matrix are, from the above analysis, integrals of the products of boundary element functions and derivatives of the Green function (3.2); they are all regular and are computed herein by means of a four-point Gauss formula. The integrals of $T_y G$ in (3.10) and $T_y(\partial G/\partial N')$ in (3.11) contain terms with logarithmic singularities at $\boldsymbol{r} = \boldsymbol{r}'$; they are evaluated by means of a four-point Berthod–Zaborowski formula. The algebraic equations are solved by means of the Fortran NAg routine F04JGF.

At each step of the iteration, (3.11) is solved on $S^{(m)}$ and the solution is inserted into (3.10), the integral being taken along $S^{(m)}$. If, at any collocation point $\boldsymbol{r}' \in S^{(m)}$, $|\psi(\boldsymbol{r}')| > \epsilon$, a new approximation $S^{(m+1)}$ is found and the process repeated.

4. Results and discussion

The method described in §3 has been used to determine the free-surface profile, S, and corresponding velocity, v_T, for a number of values of the non-dimensional parameters ψ_0, γ and α. In all cases discussed below, results were obtained from an initial free-surface approximation, $S^{(0)}$, comprising 32 uniformly-distributed collocation points; results obtained using more collocation points did not differ, to the presented accuracy, of those discussed below. In most cases, $S^{(0)}$ was taken as a circle of radius $1+\psi_0$, concentric with the cylinder. In those cases where S was expected to differ substantially from a circle (e.g. for large ψ_0), $S^{(0)}$ was taken as S calculated using a slightly smaller value of ψ_0.

The upper bound for the absolute value of the stream function at the collocation points was $\epsilon = 10^{-6}$. We observed that, depending on the parameters ψ_0, γ and α, the CPU time (on an IBM 3090/VF-180E computer) required to find S was in the range 50–70 s. Physical intuition would suggest the existence of a maximum supportable fluid load for a given rotation rate. Correspondingly, we predicted a maximum value of ψ_0

for which convergence would occur. Numerical experiments did indeed reveal that, for each value of γ, there was a maximum value of ψ_0 for which convergence could be obtained. In all cases for which convergence was found to occur, it did so in less than 100 s CPU time.

In the subsequent analysis and discussion, the fluid surface is represented (in standard polar coordinates) by $r = 1+h(\theta)$, with θ defined as in figure 1. In the event that $0 < h \ll 1$, it is to be expected that the velocity field and free-surface profile may be found using thin-film theory. This line of approach was pursued by Moffatt (1977) and Preziosi & Joseph (1988).

Let $u(r,\theta)$ and $w(r,\theta)$ be, respectively, the tangential and radial components of the fluid velocity. In keeping with the thin-film approximation, Preziosi & Joseph (1988) replace the exact, nonlinear, equation of motion by

$$\frac{\partial^2 u}{\partial r^2}+\frac{1}{r}\frac{\partial u}{\partial r}-\frac{u}{r^2}=\gamma\cos\theta. \tag{4.1}$$

They then replace the exact condition expressing the vanishing of shear stress at the free surface,

$$\tau_{r\theta}=\frac{1}{2}\left[r\frac{\partial}{\partial r}\left(\frac{u}{r}\right)+\frac{1}{r}\frac{\partial w}{\partial\theta}\right]=0 \quad \text{on } r=1+h(\theta), \tag{4.2}$$

by the approximate condition

$$\frac{\partial}{\partial r}\left(\frac{u}{r}\right)=0 \quad \text{on } r=1+h(\theta). \tag{4.3}$$

The no-slip condition on the cylinder is

$$u=1 \quad \text{on } r=1. \tag{4.4}$$

Equation (4.1) may be solved, subject to (4.3) and (4.4), to yield

$$u=r+\tfrac{1}{3}\gamma\cos\theta\left\{r^2-\left(1+\frac{(1+h)^3}{2}\right)r+\frac{(1+h)^3}{2r}\right\}. \tag{4.5}$$

If one now substitutes $r=1+\eta$ into (4.5), expands the braced term in powers of $\eta(0<\eta\ll 1)$, and omits terms of cubic and higher order in η and h, one obtains

$$u(1+\eta,\theta)=1+\eta-\tfrac{1}{2}\gamma\cos\theta\,\eta(2h-\eta), \tag{4.6}$$

in accordance with (3.1) and (3.2) of Preziosi & Joseph (1988). We mention that, to this order in γ and h, (4.6) also arises if (4.1) is replaced by the simpler equation

$$\frac{\partial^2 u}{\partial r^2}=\gamma\cos\theta. \tag{4.7}$$

As expected, the velocity given by (4.6) reduces to rigid-body rotation as $\gamma\to 0$ ($\nu\to\infty$).

If γ is now large, the maximum load can be expected to be so small that the corresponding layer thickness is within the region of validity of the above expression for u. When using (4.6) to find the maximum load, Preziosi & Joseph (1988) therefore neglect the term η, thereby obtaining the same expression for u as given in Moffatt (1977).

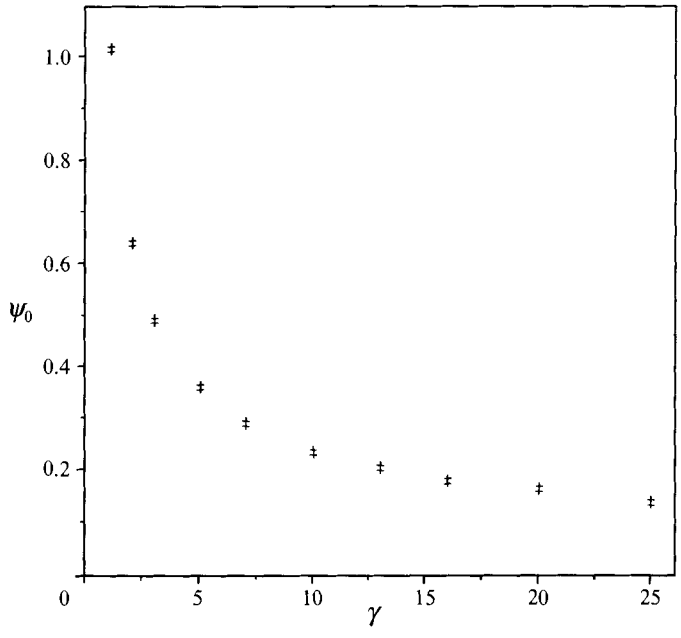

FIGURE 2. The maximum fluid flux, ψ_0, as a function of the parameter γ. For each value of γ, the lower cross denotes $\hat{\psi}_0$, the largest value of ψ_0 for which a converged surface profile could be found; the upper cross denotes $\check{\psi}_0$, the smallest value for which no such convergence was observed.

From (4.6) an approximation to ψ_0, the total flux, is obtained by radial integration of u across the fluid layer:

$$\psi_0 = \int_0^h u \, \mathrm{d}\eta = h + \tfrac{1}{2}h^2 - \tfrac{1}{3}\gamma \cos\theta \, h^3. \tag{4.8}$$

Since ψ_0 is a constant, (4.8) expresses the fact that (in the thin-film approximation) h must be weakly dependent on θ. In the limit of small h, and hence small ψ_0, we solve (4.8) for h by representing h as a power series in ψ_0 and equating coefficients. We find that, to third order in ψ_0,

$$h = \psi_0 - \tfrac{1}{2}\psi_0^2 + [\tfrac{1}{3}\gamma \cos\theta + \tfrac{1}{2}]\,\psi_0^3. \tag{4.9}$$

The main point to observe from (4.9) is that, to the extent that thin-film theory is applicable, h is indeed only weakly dependent on θ, such variation as there is being only third order in ψ_0.

It is intuitively obvious that the maximum fluid mass which can be supported by the rotating cylinder is a decreasing function of γ. In order to investigate this dependency quantitatively, several series of numerical experiments were undertaken, using the integral-equation method described above. Surface tension effects were neglected by setting $\alpha = 0$. Thereafter, a series of computations, with increasing values of ψ_0, was undertaken.

As discussed above, convergence to a stationary S, when it did occur, always did so in less than 100 s CPU time. We therefore interpreted a CPU time of greater than 200 s without convergence having occurred as being indicative that the value chosen for ψ_0 was larger than that corresponding to the maximum supportable load. When such a value of ψ_0 had been reached, more detailed numerical experiments were performed to narrow the interval between a value, $\hat{\psi}_0$, for which convergence did occur, and one, $\check{\psi}_0$,

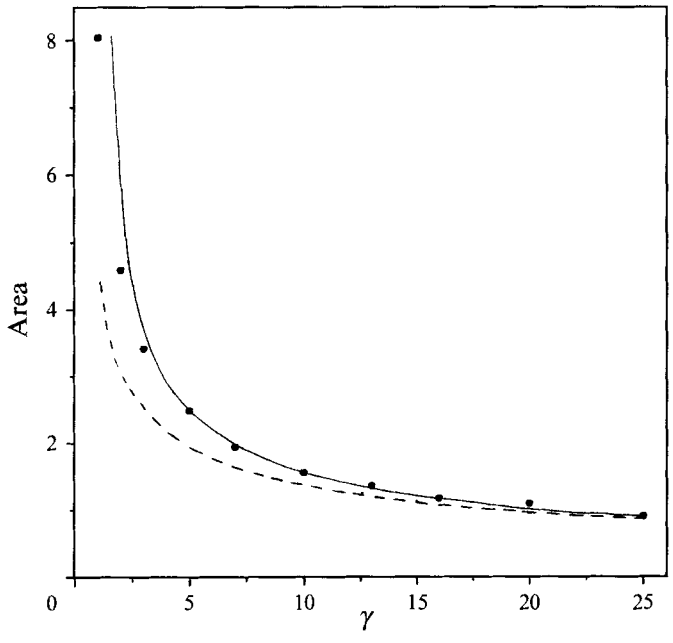

FIGURE 3. The largest non-dimensional fluid cross-section supported by the cylinder, as a function of γ. The dots correspond to the lower set of crosses in figure 2. In all cases, $\alpha = 0$. – – –, Moffatt (1977); ——, Kelmanson (1994).

for which it did not. Calculations were continued until $\check{\psi}_0 - \hat{\psi}_0 \leqslant 10^{-2}$. Figure 2 shows both $\hat{\psi}_0$ and $\check{\psi}_0$ for a range of values of γ, whilst figure 3 shows the non-dimensional area of the fluid cross-section corresponding to $\hat{\psi}_0$ over the same range. In figure 3, these areas, which correspond to maximum-supportable loads, are represented by dots; the dashed line is the maximum load predicted by Moffatt (1977); the solid line is the maximum load predicted by the theory of Kelmanson (1994). For $\gamma \geqslant 5$ (i.e. in the valid region for thin-film theory), the present results and those of Kelmanson (1994) agree, for all γ, to within a relative error of 10^{-2}.

Table 1 shows a comparison between the fluid-layer thickness evaluated using formula (4.9) with that obtained from the integral-equation procedure; the angle θ is as shown in figure 1. Note that the degree of agreement between the values is high when $\psi_0 = 0.05$, and slightly poorer when $\psi_0 = 0.1$; this is to be expected because of the assumptions underlying thin-film theory.

Table 2 shows a similar comparison for the free-surface velocity $v_T = u(1+h, \theta)$. The velocities predicted by thin-film theory were found by inserting the values of h, given by (4.9), into formula (4.6) with $\eta = h$. Once more, agreement is better, at most surface locations, for $\psi_0 = 0.05$ than for $\psi_0 = 0.1$. It is also evident that such agreement is better at $\theta = 180°$, where the fluid layer is thinnest, than at $\theta = 0$, where it is thickest; this, of course, is in complete agreement with thin-film theory.

Figures 4 and 5 (the latter of which uses different vertical scales for the plots) show, respectively, the surface profile and surface velocity distribution for $\alpha = 0$, $\gamma = 5$ and a range of values of ψ_0. Results for $\gamma = 5$ are typical of those at other γ values: the surface S is almost circular and concentric with the cylinder until ψ_0 is close to $\hat{\psi}_0$ which, for this value of γ, is 0.355.

The free-surface velocity is, of course, greater on the side where the motion is in the direction of gravity than on the side where it is opposed by gravity. As expected, for

$\alpha = 0$	$\gamma = 1$	$\psi_0 = 0.05$	$\alpha = 0$	$\gamma = 1$	$\psi_0 = 0.10$
θ	h^*	h	θ	h^*	h
0	0.04885	0.04887	0	0.09583	0.09575
45	0.04884	0.04885	45	0.09574	0.09566
90	0.04881	0.04883	90	0.09550	0.09545
135	0.04878	0.04880	135	0.09526	0.09524
180	0.04877	0.04879	180	0.09517	0.09515
225	0.04878	0.04880	225	0.09526	0.09524
270	0.04881	0.04883	270	0.09550	0.09545
315	0.04884	0.04885	315	0.09574	0.09566

$\alpha = 0$	$\gamma = 5$	$\psi_0 = 0.05$	$\alpha = 0$	$\gamma = 5$	$\psi_0 = 0.10$
θ	h^*	h	θ	h^*	h
0	0.04902	0.04903	0	0.09717	0.09702
45	0.04896	0.04897	45	0.09668	0.09654
90	0.04881	0.04883	90	0.09550	0.09545
135	0.04867	0.04869	135	0.09432	0.09442
180	0.04860	0.04863	180	0.09383	0.09402
225	0.04867	0.04869	225	0.09432	0.09442
270	0.04881	0.04883	270	0.09550	0.09545
315	0.04896	0.04897	315	0.09668	0.09654

TABLE 1. The fluid film thickness found from thin-film theory, $h^*(\theta)$, and numerically, $h(\theta)$, for various parameter values

$\alpha = 0$	$\gamma = 1$	$\psi_0 = 0.05$	$\alpha = 0$	$\gamma = 1$	$\psi_0 = 0.10$
θ	v_T^*	v_T	θ	v_T^*	v_T
0	1.0477	1.0462	0	1.0912	1.0888
45	1.0480	1.0465	45	1.0925	1.0903
90	1.0488	1.0474	90	1.0955	1.0938
135	1.0496	1.0483	135	1.0985	1.0973
180	1.0500	1.0487	180	1.0997	1.0987
225	1.0496	1.0483	225	1.0985	1.0973
270	1.0488	1.0474	270	1.0955	1.0938
315	1.0480	1.0465	315	1.0925	1.0903

$\alpha = 0$	$\gamma = 5$	$\psi_0 = 0.05$	$\alpha = 0$	$\gamma = 5$	$\psi_0 = 0.10$
θ	v_T^*	v_T	θ	v_T^*	v_T
0	1.0430	1.0411	0	1.0736	1.0683
45	1.0447	1.0430	45	1.0802	1.0760
90	1.0488	1.0474	90	1.0955	1.0938
135	1.0529	1.0518	135	1.1101	1.1108
180	1.0545	1.0536	180	1.1159	1.1177
225	1.0529	1.0518	225	1.1101	1.1108
270	1.0488	1.0474	270	1.0955	1.0938
315	1.0447	1.0430	315	1.0802	1.0760

TABLE 2. The free-surface tangential velocity found from thin-film theory, $v_T^*(\theta)$, and numerically, $v_T(\theta)$, for various parameter values

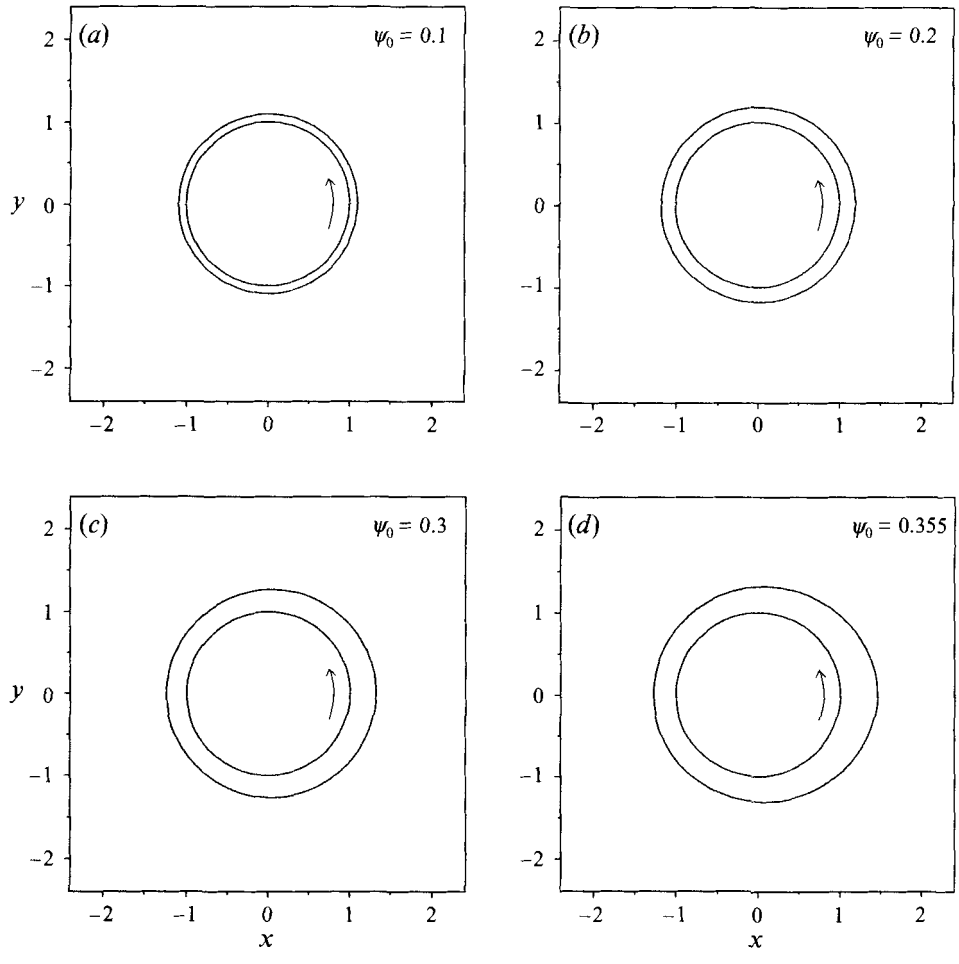

FIGURE 4. The stationary free-surface profile for $\alpha = 0$, $\gamma = 5$ and $\psi_0 = 0.1$, 0.2, 0.3 or 0.355.

$\psi_0 = 0.1$, the velocity distribution predicted by thin-film theory agrees well with that given by the numerical solution; this agreement deteriorates as ψ_0 increases. It is interesting to note that, in all cases examined, thin-film theory underestimates the variation in free-surface velocity and that, for all values of ψ_0, the approximation is better at $\theta = 180°$, where the fluid layer is of minimum thickness, than it is at $\theta = 0$, where the layer attains its maximum thickness. It is also noteworthy that, even for $\psi_0 = 0.3$, where the fluid mass is 79% of that supportable with $\hat{\psi}_0 = 0.355$, the lowest value of the free-surface velocity is only slightly less than that at the cylinder surface.

Plots of the surface profile and velocity distribution for other values of γ (and the corresponding value of ψ_0) are given in figures 6 and 7. Of all cases considered, the surface profile in figure 6(*a*) ($\gamma = 1$, $\psi_0 = \hat{\psi}_0 = 1.010$) displayed the greatest deviation from a circle; its corresponding velocity distribution is shown in figure 6(*b*). In the profile of figure 7(*a*) ($\psi = 2$, $\psi_0 = \hat{\psi}_0 = 0.635$), the layer thickness at $\theta = 0$ is smaller than the corresponding one in figure 6(*a*), and so it is somewhat surprising that the surface velocity at $\theta = 0$ (see figure 7*b*) is less than that shown in figure 6(*b*). This implies that, even for large supported fluid masses, the rigid-body effect, represented in thin-film theory by the linear term, η, in (4.6), is still important in comparison with the gravity effect, represented in thin-film theory by the term $-\frac{1}{2}\gamma \cos\theta \eta^2$.

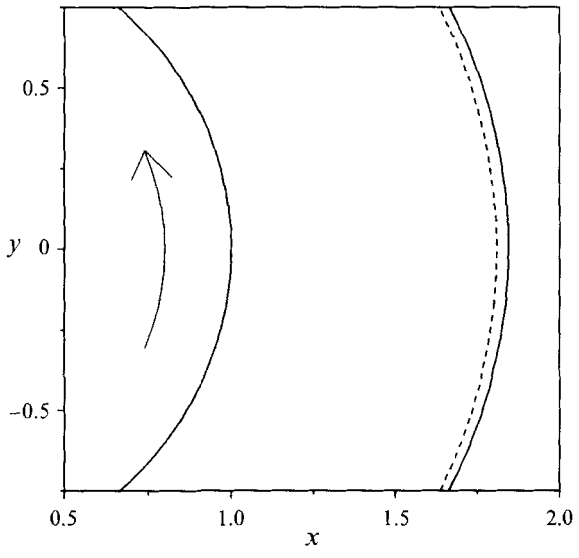

FIGURE 8. Expanded detail, near $\theta = 0$, of stationary free-surface profiles for $\gamma = 1$ and $\psi_0 = 0.9$; ——, $\alpha = 0$; – – – –, $\alpha = 100$.

$\alpha = 0$	$\gamma = 1$	$\psi_0 = 0.9$
θ	h	v_T
0	0.844727887709640	1.2853
45	0.784172630374174	1.3910
90	0.687661104747609	1.6191
135	0.627275505539659	1.8090
180	0.608174135735756	1.8781
225	0.627275505539659	1.8090
270	0.687661104747609	1.6191
315	0.784172630374174	1.3910

TABLE 3. Fluid film thickness, $h(\theta)$, and free-surface tangential velocity, $v_T(\theta)$, for $\alpha = 0$, $\gamma = 1$ and $\psi_0 = 0.9$

$\alpha = 100$	$\gamma = 1$	$\psi_0 = 0.9$
θ	h	v_T
0	0.808971357855722	1.3437
45	0.772846196755399	1.4178
90	0.698743060359047	1.5950
135	0.629343045091761	1.8020
180	0.599491825167775	1.9057
225	0.627079025855326	1.8078
270	0.702029318255682	1.5860
315	0.779970779509766	1.4043

TABLE 4. Fluid film thickness, $h(\theta)$, and free-surface tangential velocity, $v_T(\theta)$, for $\alpha = 100$, $\gamma = 1$ and $\psi_0 = 0.9$

very small. Figure 8 displays the fact that, even if a large surface-tension effect is incorporated, the surface profile remains close to being symmetric about the x-axis. However, the fact that surface tension does indeed break the symmetry is reflected in table 4, which shows numerical results $h(\theta)$ and $v_T(\theta)$ for the parameters $\alpha = 100$, $\gamma = 1$ and $\psi_0 = 0.9$: if one compares tables 3 and 4, symmetry of results has disappeared when α is non-zero.

The authors wish to express their gratitude to both Professor Kaj Madsen, for making the subroutine MIOINF available to them, and to Professor H. K. Moffatt, for bringing to their attention the paper by Preziosi and Joseph.

Appendix

In the absence of surface tension ($\alpha \equiv 0$), the solution of the boundary-value problem represented by (2.4) to (2.6) has the following properties: the stream function is an even function of y; the pressure is an odd function of y; the free surface is symmetric about the x-axis. We now prove this assertion.

Let the annular region Ω be bounded within by the unit circle, C (centred at the origin), and without by the closed curve, S, and let $\partial\Omega = C \cup S$. Let Ω_R and S_R be, respectively, the reflections, in the x-axis, of the region Ω and its outer boundary S, and let $\partial\Omega_R = C \cup S_R$. Furthermore, let $\boldsymbol{T}$ and $\boldsymbol{N}$ be a left-handed pair of orthogonal, unit vectors at either $(x, y) \in \Omega$ or $(x, -y) \in \Omega_R$, and let $\boldsymbol{N}$ be the unit inward normal on C. Figure 9 depicts the geometry so far described.

Let the functions $p = p(x, y)$ and $\psi = \psi(x, y)$ satisfy the following boundary-value problem on $\Omega \cup \partial\Omega$:

$$\frac{\partial p}{\partial x} = \frac{\partial \Delta\psi}{\partial y}, \quad \frac{\partial p}{\partial y} = -\frac{\partial \Delta\psi}{\partial x} - \gamma \quad \text{in } \Omega, \tag{A 1}$$

$$\psi(x, y) = \psi_0, \quad \frac{\partial \psi}{\partial N} = 1 \quad \text{on } C, \tag{A 2}$$

$$\psi = 0, \quad \Delta\psi = 2\frac{\partial^2 \psi}{\partial T^2}, \quad -p + 2\frac{\partial^2 \psi}{\partial N \partial T} = 0 \quad \text{on } S. \tag{A 3}$$

Consider now the functions $q = q(x, y)$ and $\phi = \phi(x, y)$ defined by

$$q(x, y) \equiv -p(x, -y), \quad \phi(x, y) \equiv \psi(x, -y), \ (x, -y) \in \Omega \cup \partial\Omega. \tag{A 4}$$

If $(x, y) \in \Omega_R$ then $(x, -y) \in \Omega$, and so (A 1) and (A 4) imply that

$$\frac{\partial q}{\partial x}(x, y) = -\frac{\partial p}{\partial x}(x, -y) = -\frac{\partial \Delta\psi}{\partial y}(x, -y) = \frac{\partial \Delta\phi}{\partial y}(x, y). \tag{A 5}$$

Similarly,

$$\frac{\partial q}{\partial y}(x, y) = \frac{\partial p}{\partial y}(x, -y) = -\frac{\partial \Delta\psi}{\partial x}(x, -y) - \gamma = -\frac{\partial \Delta\phi}{\partial x}(x, y) - \gamma. \tag{A 6}$$

(A 5) and (A 6) state that q and ϕ satisfy the Stokes equations in Ω_R. Now let $(x, y) \in C$; then $(x, -y) \in C$ and (A 2) implies that

$$\phi(x, y) = \psi(x, -y) = \psi_0, \tag{A 7}$$

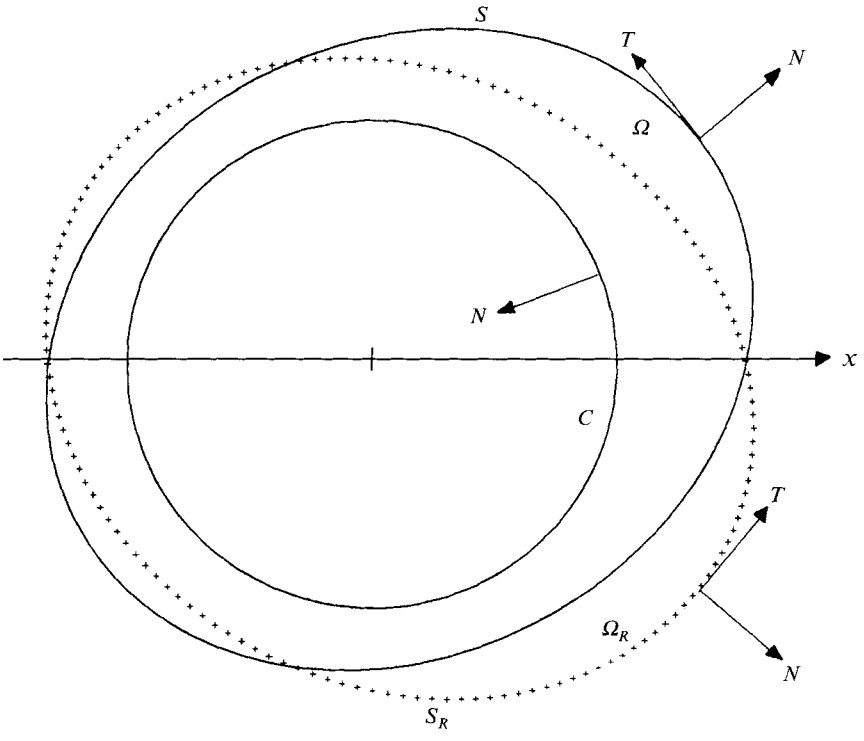

FIGURE 9. Schematic flow region and its reflection in the x-axis.

and
$$\frac{\partial\phi}{\partial N}(x,y) = \left\{N_x\frac{\partial\phi}{\partial x}+N_y\frac{\partial\phi}{\partial y}\right\}_{(x,y)}$$
$$= \left\{N_x\frac{\partial\psi}{\partial x}+(-N_y)\left(-\frac{\partial\psi}{\partial y}\right)\right\}_{(x,-y)} = \frac{\partial\psi}{\partial N}(x,-y) = 1. \tag{A 8}$$

So, ϕ satisfies boundary conditions (A 2) on C. If now $(x,y)\in S_R$ then $(x,-y)\in S$. Therefore, by the first of (A 3),

$$\phi(x,y) = \psi(x,-y) = 0. \tag{A 9}$$

Moreover, using (A 4), we have

$$\Delta\phi(x,y)-2\frac{\partial^2\phi}{\partial T^2}(x,y)$$
$$= \Delta\phi(x,y)-2\left\{T_x^2\frac{\partial^2\phi}{\partial x^2}+2T_xT_y\frac{\partial^2\phi}{\partial x\,\partial y}+T_y^2\frac{\partial^2\phi}{\partial y^2}\right\}_{(x,y)}$$
$$= \Delta\psi(x,-y)-2\left\{T_x^2\frac{\partial^2\psi}{\partial x^2}+2(-T_x)T_y\left(-\frac{\partial^2\psi}{\partial x\,\partial y}\right)+T_y^2\frac{\partial^2\psi}{\partial y^2}\right\}_{(x,-y)}$$
$$= \Delta\psi(x,-y)-2\frac{\partial^2\psi}{\partial T^2}(x,-y) = 0, \tag{A 10}$$

by the second of (A 3), since $(x, -y) \in S$. Again using (A 4), we have

$$\begin{aligned}
&-q(x,y)+2\frac{\partial^2\phi}{\partial N\,\partial T}(x,y)\\
&\quad=-q(x,y)+2\left\{N_x T_x\frac{\partial^2\phi}{\partial x^2}+(N_x T_y+N_y T_x)\frac{\partial^2\phi}{\partial x\,\partial y}+N_y T_y\frac{\partial^2\phi}{\partial y^2}\right\}_{(x,y)}\\
&\quad=p(x,-y)+2\left\{N_x(-T_x)\frac{\partial^2\psi}{\partial x^2}+(N_x T_y+(-N_y)(-T_x))\left(-\frac{\partial^2\psi}{\partial x\,\partial y}\right)\right.\\
&\qquad\left.+(-N_y)T_y\frac{\partial^2\psi}{\partial y^2}\right\}_{(x,-y)}\\
&\quad=p(x,-y)-2\frac{\partial^2\psi}{\partial N\,\partial T}(x,-y)=0,
\end{aligned}\tag{A 11}$$

by the third of (A 3), since $(x, -y) \in S$.

We have so far shown that, if the set $\{p, \psi, S\}$ is a solution of the free boundary-value problem, so is the set $\{q, \phi, S_R\}$. The Stokes flow under consideration ($\psi_0 > 0$, $R \equiv 0$, $\alpha \equiv 0$) is a particular case of a more general class of flows ($\psi_0 > 0$, $R \geqslant 0$, $\alpha \geqslant 0$) to which the existence-uniqueness theorem of Pukhnachev (1977) may be applied. Therefore, the solution of our boundary-value problem is unique, and the two sets described above must be identical. Thus, the pressure field is antisymmetric about the x-axis,

$$p(x,y) = -p(x,-y), \tag{A 12}$$

the stream function is symmetric about the x-axis,

$$\psi(x,y) = \psi(x,-y), \tag{A 13}$$

and the free surface S is symmetric about the x-axis.

REFERENCES

HANSEN, E. B. 1987 Stokes flow down a wall into an infinite pool. *J. Fluid Mech.* **178**, 243–256.

KELMANSON, M. A. 1994 Theoretical and experimental analyses of the maximum-supportable fluid load on a rotating cylinder. Submitted.

MADSEN, K. 1975 An algorithm for minimax solution of overdetermined systems of non-linear equations. *J. Inst. Maths Applics* **16**, 321–328.

MADSEN, K., HEGELUND, P. & HANSEN, P. C. 1991 Fortran non-gradient subroutines for non-linear optimisation. *Rep. NI-91-05*, Numerical Institute, Technical University of Denmark, DK-2800 Lyngby, Denmark.

MALONE, B. 1992 An experimental investigation of roll-coating phenomena. PhD thesis, Department of Mechanical Engineering, University of Leeds, Leeds LS2 9JT, UK.

MOFFATT, H. K. 1977 Behaviour of a viscous film on the outer surface of a rotating cylinder. *J. Méc.* **16**, 651–673.

PREZIOSI, L. & JOSEPH, D. D. 1988 The run-off condition for coating and rimming flows. *J. Fluid Mech.* **187**, 99–113.

PUKHNACHEV, V. V. 1974 Problems with a free boundary for the Navier–Stokes equations. PhD thesis (in Russian), Lavrenteyev Institute of Hydrodynamics, Novosibirsk, USSR.

PUKHNACHEV, V. V. 1977 Motion of a liquid film on the surface of a rotating cylinder in a gravitational field (in Russian). *Z. Prikl. Mekh. i Tekh. Fiz.* **3**, 78–88. English translation in (1977), *J. Appl. Mech. Tech. Phys.* **18**, 344–351.

THOMPSON, H. M. 1992 A theoretical investigation of roll-coating phenomena. PhD thesis, Department of Applied Mathematical Studies, University of Leeds, Leeds LS2 9JT, UK.